Journal of Solid State Chemistry 211 (2014) 130–135

Contents lists available at ScienceDirect

Journal of Solid State Chemistry

journal homepage: www.elsevier.com/locate/jssc

# Synthesis, characterization and magnetic properties of a manganese (II) silicate containing frustrated $S=5/2$ zig–zag ladders

P. Brandão [a,*], A.M. dos Santos [b], L.S. Paixão [c], M.S. Reis [c]

[a] Departamento de Química/CICECO, Universidade de Aveiro, 3810-193 Aveiro, Portugal
[b] Quantum Condensed Matter Division, Neutron Sciences Directorate, Oak Ridge National Laboratory, Oak Ridge, TN 37831-6475, USA
[c] Instituto de Física, Universidade Federal Fluminense, Av. Gal. Milton Tavares de Souza s/n, 24210-346 Niterói, RJ, Brazil

ARTICLE INFO

*Article history:*
Received 7 October 2013
Received in revised form
13 December 2013
Accepted 16 December 2013
Available online 24 December 2013

*Keywords:*
Hydrothermal synthesis
Serandite mineral
Manganese silicate
Magnetic chain

ABSTRACT

The hydrothermal synthesis, structural characterization and magnetic properties of a manganese silicate with ideal formula of $NaMn_2Si_3O_8(OH)$ is reported. This compound is a synthetic analog to the naturally occurring mineral Serandite. The crystal structure comprises $MnO_6$ octahedra and $SiO_4$ tetrahedra. The $MnO_6$ share four edges with neighboring octahedra forming double chains. These chains are connected by silicate chains $Si_3O_8(OH)$ resulting in an open framework structure with six-member ring channels where sodium ions are located. From the magnetic point of view, the intra-chain exchange between neighboring $S=5/2$ manganese ions is weak, partly due to the distortion observed in the octahedra, but also due to the frustrated topology of the chain. A successful fitting of the magnetic susceptibility was obtained by considering a double chain numerical model with Monte Carlo derived empirical parameters.



## 1. Introduction

Transition metal silicates are framework solids comprising corner sharing $SiO_4$ tetrahedra, combined with transition metals that can occur in a variety of coordination environments, oxidation states and metal–metal connectivities. Given the structural and chemical versatility of this class of materials, it is no surprise that they are at the base of a fertile field of research that shows promise in areas as diverse as catalysis, ion exchangers, gas absorption and even phosphors [1,2].

When synthesized with magnetically active transition metals, such frameworks often exhibit exotic magnetic properties that are primarily related to low dimensional magnetism (clusters [3], chains [4] and layers [5]) as well as frustration [6]. Furthermore, these systems represent a compromise between three dimensional bulk systems (with strong metal–metal exchange interaction and the corresponding elevated ordering temperatures), and organic-based coordination polymers, where exchange is much weaker – few K or less – and poorer chemical and thermal stability (for a review see Ref. [7]).

It is well known that the structures that result from the hydrothermal synthesis of transition metal silicates are tremendously sensitive to synthesis conditions [8], yielding frequently either novel structural types or mimicking natural processes, resulting in compounds analogous to naturally occurring minerals, but with controlled compositions.

As a result of a systematic study aimed at finding novel metal silicates with exotic magnetic properties, we successfully synthesized hydrothermally one manganese silicate isostructural with the Serandite mineral. This mineral was first described by Lacroix in 1931 [9]. In 1976, Takéuchi and co-workers, using a crystal from Tanohata mine, Japan, determined its structure by single crystal X-ray diffraction [10]. This compound has the idealized formula $Na(Mn_{2-x}Ca_x)_1Si_3O_8(OH)$ $(0\leq x\leq 2)$ and crystalizes in the triclinic system, space group $P\bar{1}$ with cell parameters $a=7.683(1)$ Å, $b=6.889(1)$ Å, $c=6.747(1)$ Å, $\alpha=90.53(1)^\circ$, $\beta=94.12(2)^\circ$, $\gamma=102.75(2)^\circ$, $V=451.2(6)$ Å$^3$ and $Z=2$. This structure type forms a solid solution between the manganese rich end member Serandite (where the $Mn^{+2}$ oxidation state confers a very attractive pink color to natural specimens), and the calcium rich Pectolite, $NaCa_2Si_3O_8(OH)$ [11]. The crystal structures of the minerals Pectolite–Serandite series are built of double chains of edge-sharing $MnO_6$ or $CaO_6$ octahedra running parallel to $b$ axis, which are linked by silicate chains of $SiO_8(OH)$ units also along $b$ direction. These double chains are similar to those observed in Hollandite ($Ba(Mn^{4+}, Mn^{3+})_8O_{16}$) and Ramsdellite ($Mn^{2+}O_2$), but with the important difference that here the chains are isolated and all manganese ions are in the 2+ oxidation state, yielding a spin $S=5/2$, making it an interesting model compound for a frustrated chain with classical spin. A comparative view of the double chain stacking arrangement in Hollandite, Ramsdellite and Serandite is depicted in Fig. 1.

Structurally, this mineral series shows two peculiar characteristics: one is related to the preferential distribution of Ca and Mn

* Corresponding author.
*E-mail address:* pbrandao@ua.pt (P. Brandão).

0022-4596/$ - see front matter © 2013 Elsevier Inc. All rights reserved.
http://dx.doi.org/10.1016/j.jssc.2013.12.013

over the two available metal positions; and the other is the presence of a strongly asymmetric hydrogen bond O–H···O. These features are behind the number of structural work around the mineral series [12–14]. So far, to the best of our knowledge, the magnetic study of this manganese silicate is not reported. In the present work, the hydrothermal synthesis, structural characterization and magnetic properties of the synthetic analog of the Serandite mineral are presented.

## 2. Experimental section

### 2.1. Synthesis

The manganese silicate was synthesized hydrothermally under autogenous pressure. Chemicals were purchased from commercial sources and used without further purification: sodium silicate solution ($Na_2O$ 8 wt%, $SiO_2$ 27 wt%, Merck); NaOH (Pronalab), KCl (Panreac) and $Mn(SO_4)\cdot 4H_2O$ (Merck). A typical synthesis was made by mixing 7.45 g of $H_2O$ and 2.01 g of $Mn(SO_4)\cdot 5H_2O$. A second solution was obtained by mixing 6.89 g of a sodium silicate solution, 7.85 g of $H_2O$, 1.50 g of NaOH and 0.99 g of KCl. These two solutions were mixed and stirred thoroughly until an homogeneous gel was obtained. This was then sealed in Teflon lined autoclaves and heated at 230 °C for 7 days. After this, the autoclaves were cooled under running water and the reaction products were filtered yielding a pink powder, which was washed and dried at room temperature.

### 2.2. Characterization

Powder X-ray diffraction (XRD) data were collected at room temperature on a Philips X′pert diffractometer with a curved graphite monochromator (Cu-*K*α radiation), in a Bragg–Brentano para-focusing optics configuration. The sample was step-scanned in 0.02° 2$\theta$ steps with a counting time of 50 s per step. Scanning Electron Microscopy (SEM) images were recorded on a Hitachi S-4100 Field Emission Gun tungsten filament working with a voltage of 25 kV. The chemical composition was determined by energy dispersive analysis of X-rays (EDAX). Termogravimetry (TGA) was measured with TGA-50 Shimadzu analyzer. The sample was heated under air at a rate of 5 °C/min from room temperature to 700 °C. FTIR spectra were recorded in transmittance mode on a Mattson Mod 7000 spectrophotometer, pelletized in KBr, in the range 250–4000 $cm^{-1}$. The pellets were prepared by sample dispersion (0.2 mg) in a KBr matrix (150 mg) and pressed. The spectra were obtained by averaging 128 scans with 4 $cm^{-1}$ resolution.

Magnetic measurements were performed in a commercial Quantum Design SQUID magnetometer.

## 3. Results and discussion

### 3.1. Physical characterization

Electron microscopy of the recovered samples, shown in Fig. 2, reveals a morphology in the form of long needles with irregular size. Such very anisotropic crystal morphology is a normal occurrence when using solution-based synthesis methods, particularly in cases – such as this one – where the structure itself presents structurally a strong one-dimensional character. In fact, even natural specimens of Serandite and its isostructural counterpart Pectolite, have been found that exhibit a radiant acicular habit, elongated along [010], reminiscent of the reaction product presented here. The X-ray powder diffraction spectrum was also collected and is presented in Fig. 3. It should be noted that this crystal morphology favors the occurrence of preferential orientation and anisotropic peak broadening and, consequently, precludes the refinement of the structure by diffraction methods (powder and single crystal). Nonetheless a LeBail fit of the measured powder pattern was performed, using as starting values those found in the JCPDS card 04-011-5175, corresponding to the naturally occurring mineral Serandite. For this fit, 17 refinable parameters were used: scale, six lattice parameters, one offset term, a six coefficient polynomial background and a pseudo-Voight peak shape function

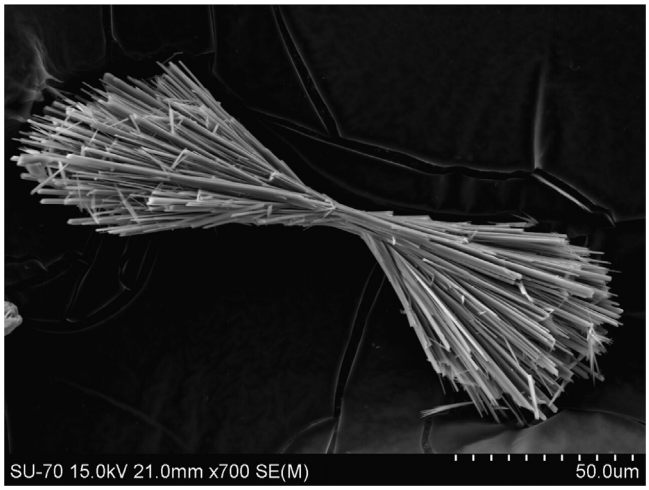


**Fig. 2.** SEM image of synthetic Serandite – $NaMn_2Si_3O_8(OH)$.

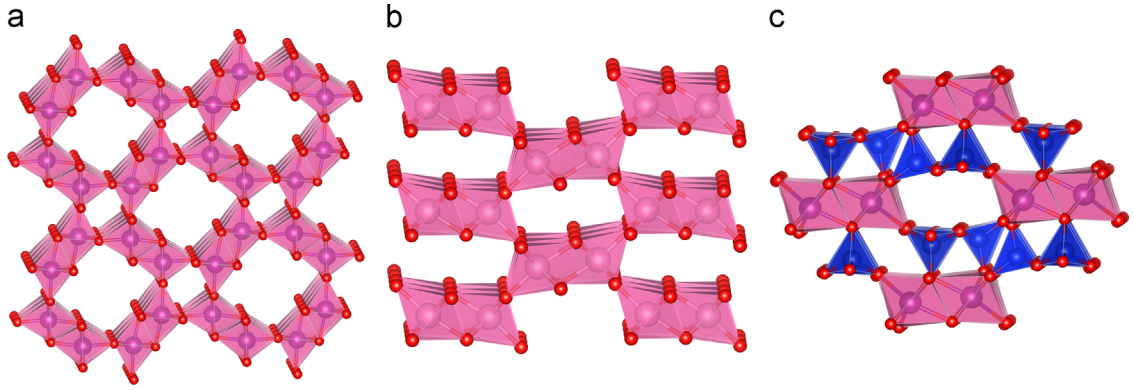


**Fig. 1.** Polyhedral representation of the $MnO_2$ chain arrangement present in (a) Hollandite; (b) Ramsdellite and (c) Serandite. The barium, sodium and hydrogen ions in Hollandite and Pectolite respectively are omitted for clarity. Mn – pink, Si – blue and O – red. (For interpretation of the references to color in this figure legend, the reader is referred to the web version of this article.)

with three refinable parameters. This resulted in a quality of fit $R=2.47\%$ and a $\chi^2=2.78$, with lattice parameters $a=7.708(3)$ Å, $b=6.890(8)$ Å, $c=6.740(1)$ Å, $\alpha=89.87(3)^\circ$, $\beta=94.22(2)^\circ$ and $\gamma=102.91(1)^\circ$. This refinement indicates that this sample is almost single phase, with a small impurity peak (of an unidentified phase) visible at $\sim 33^\circ$ $2\theta$. Energy-dispersive X-ray spectroscopy analyses of different crystals show that the synthesized sample possesses Si/Mn and Si/Na ratios of 1.62 and 2.98, respectively, which are compatible with the idealized formula for this mineral $NaMn_2Si_3O_8(OH)$ [10] (see Table 1). No other phases rich in silicon or manganese were detected.

The brief structural description that follows is intended for a better framing of the magnetic results discussed in Section 3.2, and is based on the crystallographic data published earlier [10,12,14].

The asymmetric unit of this manganese silicate is composed of two independent $Mn^{2+}$ ions, three $Si^{4+}$ atoms, and one $Na^{+}$ ion leading to the molecular formula $NaMn_2Si_3O_8(OH)$. Both symmetry independent manganese cations are octahedrally coordinated with oxygen atoms. The two $MnO_6$ octahedra share three edges giving rise to infinite double chains running along the [010] direction, as depicted in Fig. 4(a). These chains are linked by silicate chains of $Si_3O_8(OH)$ units leading to the formation of a three dimensional framework. Six-ring channels are observed along the [010] direction, where the sodium ions are located (Fig. 5). These octahedra are somewhat distorted as is depicted in Fig. 4(b). The manganese site Mn(1) the Mn–O bond lengths vary between 2.2005 Å and 2.3500 Å and the second manganese site Mn(2) the Mn–O distances range from 2.1525 Å to 2.3500 Å. Furthermore a tilt angle on the apical O–M–O further distorts the octahedra. Due to the low symmetry of the overall crystal structure, the metal–metal distances along the chain are slightly irregular; however the chain is perfectly planar. The relevant metal–metal bond angles and lengths along the chain are depicted in Fig. 6. As mentioned in the introduction, the Pectolite–Serandite mineral series shows a strongly asymmetric hydrogen bond between O(3) and O(4) atoms separated by 2.446 Å, as can be observed in Fig. 4(b). Despite the strong asymmetric hydrogen bond, a careful study by Jacobsen and co-workers found that the proton position bonded to O(3) has about 84% occupancy and an O(4)–H distance of 1.078(3)Å, while the position bonded to O(4) has an occupancy of 16% and an O(3)–H distance of 1.07(1) Å [13].

Vibrational spectroscopy, specifically Fourier Transform infrared spectroscopy (FTIR), can be used to obtain structural information of reactive groups, such as OH present here. The FTIR

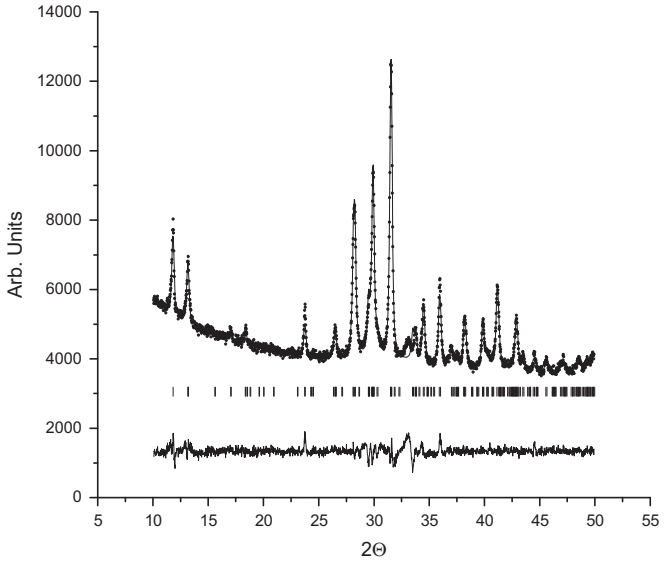


**Fig. 3.** LeBail refinement of Serandite (JCPDS card 04-011-5175). Scattered and line plots are experimental and calculated profiles respectively, vertical tick marks (|) indicate peak positions. The bottom trace depicts the difference between the experimental and calculated profiles.

**Table 1**
Chemical composition of the synthetic analog of the mineral Serandite obtained by EDS and the theoretical values.

| Chemical composition | Experimental | Theoretical |
|---|---|---|
| Si/Mn | 1.62 | 1.5 |
| Si/Na | 2.98 | 3.0 |

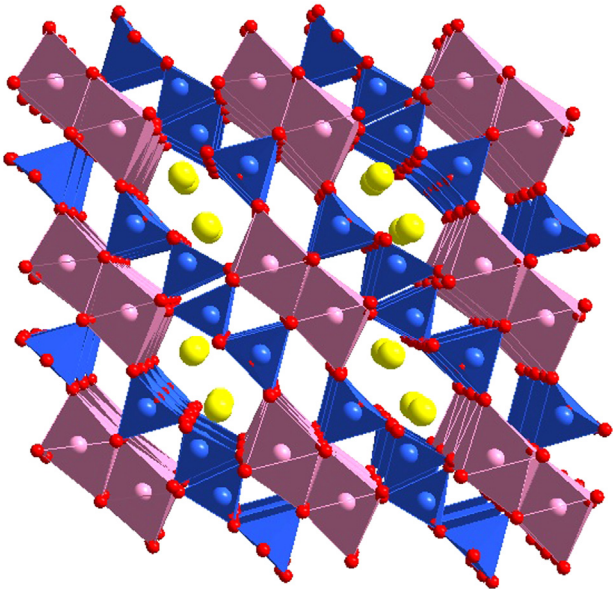

**Fig. 5.** A view of the mineral Serandite structure along [010] direction showing the six member rings. Color scheme: Mn, pink; Si, blue; O, red; Na, yellow.

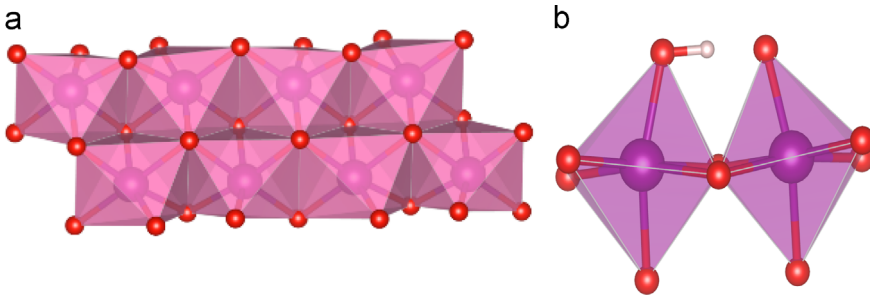


**Fig. 4.** Polyhedral representation of (a) double chains of $MnO_6$ octahedra and (b) effect of hydrogen bond on $MnO_6$ octahedra distortion. Color scheme: Mn, purple; O, red; H, white.

spectrum of the sample (Fig. 7) exhibits broad OH stretching peak around 3425 $cm^{-1}$, and sharp OH bending peak at 1383 $cm^{-1}$, these values are in accordance to those published by Hammer et al. [12], for the Serandite mineral from Mont St. Hilaire, Quebec.

The TGA presented in Fig. 8 shows that the thermal stability of this compound is remarkable: at 250 °C a small weight loss (~7%) is observed, that is consistent with de-hydrogenation, while evidence of the collapse of the crystalline structure is visible only above 600 °C.

### 3.2. Magnetic properties

The magnetic properties were studied with an ensemble of crystals and the susceptibility is presented in Fig. 9 – left axis. At 3 K a change of slope is observed, however it does not seem to develop into a magnetically ordered state down to the lowest measured temperature, in agreement with the observed magnetic isolation of the chains, inferred from the structural data. Furthermore, magnetization measurements made at 1.9 K and up to 70 kOe (inset of Fig. 9) do not show evidence of any field induced transition – that would be present if a weak inter-chain ordering would be present at that temperature. It is noteworthy that the formula unit (FU) considered in this work contains 2 Mn ions and therefore the expected saturization magnetization should be at c. a. 10 $\mu_B$, well above the experimentally observed value. Given these observations, it can be concluded that indeed this compound realizes an ideally isolated frustrated chain system with classical spin.

In order to eliminate the temperature-independent diamagnetic contribution, in the Curie–Weiss fit of the data, the temperature derivative of the magnetic susceptibility $|d\chi/dT|^{-1/2}$ was used [15](Fig. 9 – right axis). The resulting linear plot (analogous to the inverse susceptibility), allows the extraction of the paramagnetic effective moment $p_{eff}$ and the paramagnetic Curie temperature $\theta_p$. A good agreement is obtained between the experimentally obtained value of $p_{eff}=5.5(7)\ \mu_B$ and the corresponding theoretical value (estimated using $g=2$, orbital angular moment $L=0$ and spin $S=5/2$)

$$p_{eff} = g\sqrt{S(S+1)}\ \mu_B = 5.92\ \mu_B$$

is indicative of a small orbital contribution to the total angular moment for this compound. The $S=5/2$ is consistent with all Mn in a 2+ oxidation state and thus negligible mixed valences. On the other hand, the value of the paramagnetic Curie temperature $\theta p = -6.9(8)$ K is evidence that the metal exchange interaction is antiferromagnetic, consistent with the Goodenough–Kanamori rules [16,17] for edge sharing octahedra of high spin $d^5$ ions. The origin of the small magnitude of the exchange may reside on the observed extra distortion in the $MnO_6$ octahedra (beyond the expected Jahn–Teller distortion), caused by the hydrogen bonding, as highlighted in Fig. 4b.

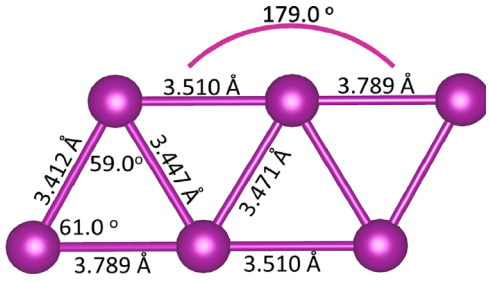


**Fig. 6.** Relevant bond angles and distances along.

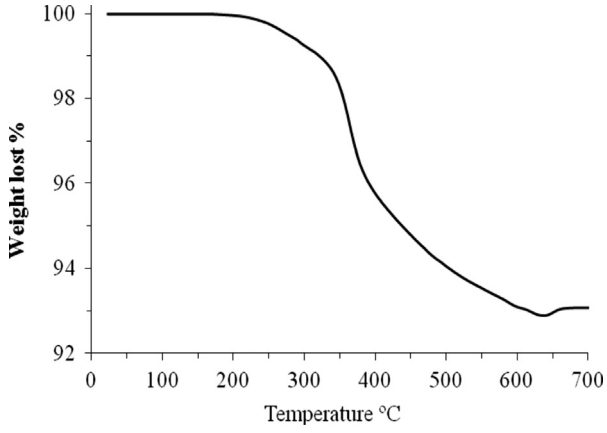


**Fig. 8.** TGA curve of manganese silicate synthetic analog of the mineral Serandite, recorded in air.

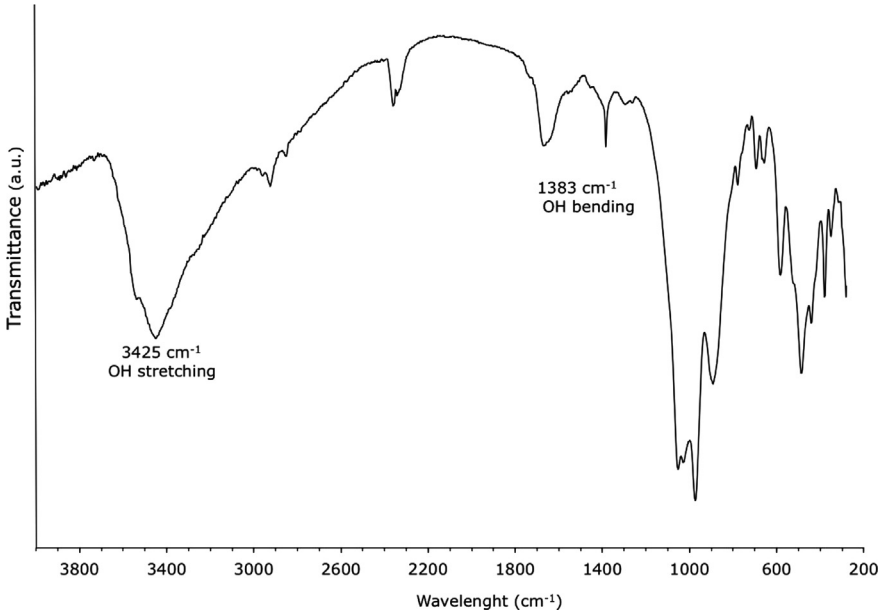


**Fig. 7.** FTIR spectrum of manganese silicate synthetic analog of the mineral Serandite.

The plot of $\chi T$ as a function of temperature, shown in Fig. 10, is also an important quantity to understand the magnetic behavior of low dimensional magnetic systems. Here it clearly shows a deviation from standard Curie–Weiss behavior, for temperatures as high as 80 K. The positive derivative at lower temperatures is consistent with an antiferromagnetic arrangement between $Mn^{2+}$ ions. Quantitatively speaking, it is possible to describe analytically the magnetic behavior of this sample as isolated double chains of Mn (see Figs. 4a and 5). The zero-field Hamiltonian can be written as

$$H = J\sum_{\langle i,j\rangle} \vec{S}^{\,i}_A \cdot \vec{S}^{\,j}_A + J_1 \sum_i \vec{S}^{\,i}_A \cdot \vec{S}^{\,i}_B \tag{3}$$

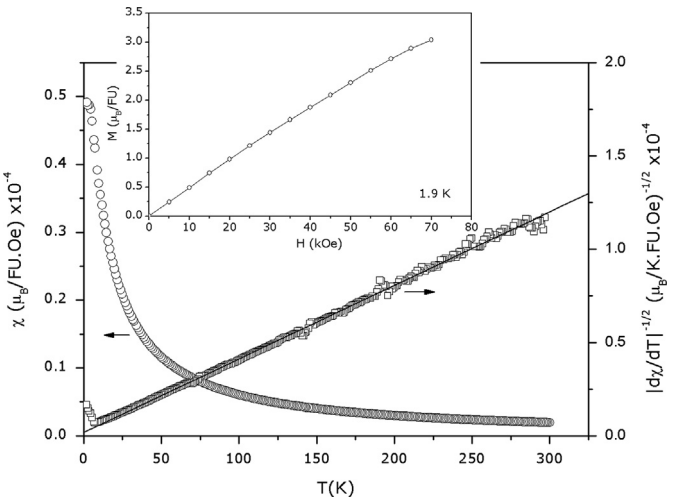


**Fig. 9.** Raw magnetic susceptibility (left) and its derivative (right), for $NaMn_2Si_3O_8(OH)$. This derivative procedure [15] removes the temperature independent contribution and then improves the estimate of $\theta p$ and $p_{eff}$. Inset: magnetization as a function of magnetic field, at 1.9 K.

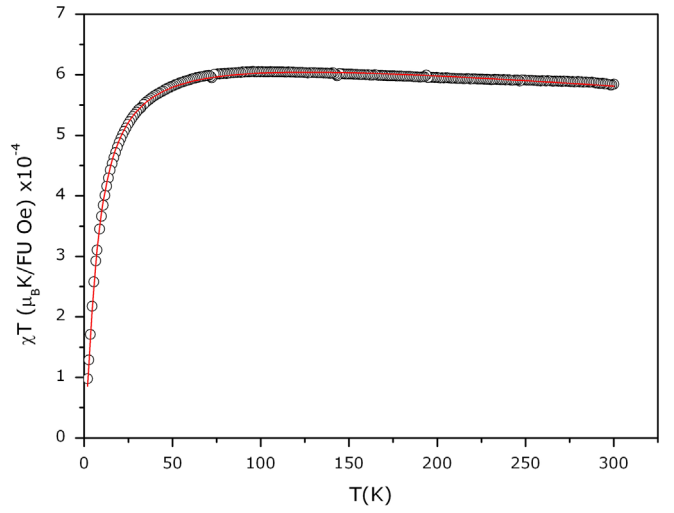


**Fig. 10.** Magnetic susceptibility times temperature as a function of temperature. Open circles: experimental data. Full line: theoretical model. Fitting parameters: $g=2.098(1)$, $J/k_B=6.28(3)$ K and $\chi_d=-2.53(2)\times10^{-7}$ $\mu_B$/FU Oe. (For interpretation of the references to color in this figure, the reader is referred to the web version of this article.)

In this sense, the result proposed by Tangoulis, for a double chain of high (classical) spins [18] is applicable. The above Hamiltonian considers a pair of double chains, namely *A* and *B*. The first summation runs over pairs of nearest-neighbor spins in double chain *A*, and the second summation represents the interaction between neighbor double chains *A* and *B*. Tangoulis used the above Hamiltonian to perform classical Monte Carlo simulations and obtained an empirical expression for the susceptibility of double chains of spin 5/2

$$\chi = \frac{g^2 S(S+1)N}{4J \quad D} \tag{4}$$

where *N* and *D* are the polynomials below. It should be noted that in this particular case $J_1 = 0$ in agreement with the description of isolated chains.

$$N = a_1 + a_2 t + a_3 t^2 + a_4 t^3 + a_5 t^4 \tag{5}$$

$$D = 1 + b_1 t + b_2 t^2 + b_3 t^3 + b_4 t^4 + b_5 t^5 \tag{6}$$

Above $t = TS(S+1)/J$. The coefficients $a_i$ and $b_i$ are listed in Table 2. Using these coefficients the susceptibility is measured in units of $\mu_B$ $FU^{-1}$ $Oe^{-1}$.

The above expression was used to fit the magnetic susceptibility measurement, as shown in Fig. 10 (red solid curve). The obtained fitting parameters are $g=2.098(1)$, $J/k_B=6.28(3)$ K and $\chi_d=-2.53(2)\times10^{-7}$ $\mu_B$/FU Oe. The value of the Landé *g* factor (near 2) is indicative of a small orbital contribution to the total angular moment; and the positive Heisenberg exchange parameter again confirms the antiferromagnetic arrangement between Mn ions. The weak interaction may explain the absence of 3D ordering in this compound, despite the high local moment available in each Mn site.

It is interesting to note that this compound shares a zig–zag chain topology with many interesting systems, namely edge sharing cuprates whose magnetic properties can be best described by a combination of near-neighbor (NN) and next-near-neighbor (NNN) interactions, also sometimes referred as $J_1$–$J_2$ chains. Examples of such systems are $CuGeO_3$[19], $Li_2CuO_2$[20] or $Rb_2Cu_2Mo_3O_{12}$[21]. A recent flurry of interest in this class of compounds arose from the discovery of magnetically induced multiferroic behavior [22]. In those examples however, the exotic behavior arises from competition between magnetic exchange in the frustrated topology compounded by the quantum spin fluctuations afforded by the spin 1/2 from copper ion in the 2+ oxidation state. By contrast, in Serandite all manganese is spin 5/2, and therefore in the classical limit, and within the experimental techniques presented here, the susceptibility can be explained across most of the temperature range with a single antiferromagnetic exchange term, and therefore not giving rise to frustration. This is evidenced by values of similar magnitude between the Curie temperature and the extracted exchange parameter along the chain. There are other examples of chains with similar topology in the chemistry of manganese, being Hollandite, mentioned earlier in the introduction, one of the most studied examples. Yet in these, despite sharing the frustrated geometry as in Serandite, the extra electronic degree of freedom afforded by the (3+)–(4+) mixed valence of manganese results in a rather high paramagnetic Curie temperature $\theta_P=-385$ K, that orders antiferromagnetically at $T_N=40$ K, but with a small ferromagnetic component. In summary, despite the absence in Serandite of the "exchange-driven"

**Table 2**
Coefficients of the polynomials in susceptibility expression.

| | | | | | |
|---|---|---|---|---|---|
| $a_i$ | $a_1 = 4.06\times10^{-2}$ | $a_2 = 6.02\times10^{-3}$ | $a_3 = -6.97\times10^{-3}$ | $a_4 = 1.2\times10^{-3}$ | $a_5 = 6.16\times10^{-4}$ |
| $b_i$ | $b_1 = 75.0$ | $b_2 = 95.1$ | $b_3 = 13.0$ | $b_4 = 11.3$ | $b_5 = 1.0$ |

frustration due to competing exchange terms, the geometric frustration compounded with the structural distortion observed in the presented compound results in a weak antiferromagnetic chain with one dimensional character down to the lowest measured temperature, making it, in this sense, a rather unique example in a class of materials already rich in physical variability.

## 4. Concluding remarks

In conclusion, we report the hydrothermal synthesis of $NaMn_2Si_3O_8(OH)$ – a manganese silicate analog with Serandite. The crystal structure comprises double chains of edge-sharing $MnO_6$ octahedra and holds promise for a prototypical high spin (in the classical limit) frustrated triangular chain. Although the lack of single crystal data precluded a more complete structural characterization, powder susceptibility measurements are indicative of weak metal–oxygen–metal super-exchange interactions, antiferromagnetic in nature, and without sign of interchain ordering down to the lowest measured temperature.

## Acknowledgment

The authors acknowledge European Union, QREN, FEDER, COMPETE, FCT, collaboration project FCT/CAPES and CICECO (pEstc/CTM/LA001/2011 for financial support). M.S.R. acknowledge Brazilian agencies: CAPES, CNPq, FAPERJ and PROPPi-UFF. Research conducted at ORNL's SNS was sponsored by the Scientific User Facilities Division, Office of Basic Energy Sciences, US Department of Energy.

Author contribution. P.B.: sample synthesis; SEM, RXD, FTIR and TG measurement and analysis. M.S.R. and L.S.P.: magnetic analysis and theoretical description. A.M.S.: magnetic measurement and analysis; structural analysis. All authors discussed results and contributed to the text of the paper.

## References

[1] S. Natarajan, S. Mandal, Angew. Chem. Int. Ed. Engl. 47 (2008) 4798–4828.
[2] R.E. Morri, P.S. Wheatley, Angew. Chem. Int. Ed. Engl. 47 (2008) 4966–4981.
[3] P. Brandão, J. Rocha, M.S. Reis, A.M. dos Santos, R. Jin, J. Solid State Chem. 182 (2009) 253–258.
[4] A.M. dos Santos, V.S. Amaral, P. Brandão, F.A. Almeida Paz, J. Rocha, L. P. Ferreira, M. Godinho, O. Volkova, A. Vasiliev, Phys. Rev. B 72 (2005) 092403.
[5] C. Gueho, D. Gianquinta, J.L. Mansot, T. Ebel, P. Palvadeau, Chem. Mater. 7 (3) (1995) 486.
[6] S. Ghose, A.W. Hewat, M. Pinkney, Solid State Commun. 74 (5) (1990) 413.
[7] J. Mrozinski, Coord. Chem. Rev. 249 (21–22) (2005) 2534.
[8] N.V. Chukanov, I.V. Pekov, R.K. Rastsvetaeva, Usp. Khim. 73 (3) (2004) 227.
[9] À. Lacroix, J. C. R. Acad. Sci. 192 (1931) 189–194.
[10] Y. Takéuchi, Y. Kudoh, T. Yamanaka, Am. Miner. 61 (1976) 229–237.
[11] M.J. Buerger, Z. Kristallogr. 108 (1956) 248.
[12] V.M.F. Hammer, E. Libowitzky, G.R. Rossman, Am. Miner. 83 (1998) 569.
[13] S.D. Jacobsen, J.R. Smith, R.J. Swope, R.I. Sheldon, Am. Miner. 85 (2000) 745–752.
[14] A. Arakcheeva, P. Pattison, N. Meisser, G. Chapuis, I. Pekov, P. Thélin, Z. Kristallogr. 222 (2007) 696–704.
[15] M.S. Reis, Fundamentals of Magnetism, Elsevier, New York, 2013.
[16] J.B. Goodenough, J. Phys. Chem. Solids 6 (1958) 287;
J.B. Goodenough, A.L. Loeb, Phys. Rev. 98 (2) (1955) 391.
[17] J. Kanamori, J. Phys. Chem. Solids 10 (2–3) (1959) 87.
[18] V. Tangoulis, Chem. Phys. 332 (2007) 271.
[19] G. Castilla, S. Chakravarty, V.J. Emery, Phys. Rev. Lett. 75 (1995) 1823;
J. Riera, A. Dobry, Phys. Rev. B 51 (1995) 16098.
[20] Y. Mizuno, T. Tohyama, S. Maekawa, T. Osafune, N. Motoyama, H. Eisaki, S. Uchida, Phys. Rev. B 57 (1998) 5326.
[21] M. Hase, H. Kuroe, K. Ozawa, O. Suzuki, H. Kitazawa, G. Kido, T. Sekine, Phys. Rev. B 70 (2004) 104426.
[22] S. Park, Y.J. Choi, C.L. Zhang, S.-W. Cheong, Phys. Rev. Lett. 98 (2007) 057601;
S. Seki, Y. Yamasaki, M. Soda, M. Matsuura, K. Hirota, Y. Tokura, Phys. Rev. Lett. 100 (2008) 127201.